ROYAL SOCIETY OPEN SCIENCE

rsos.royalsocietypublishing.org

Research

Article submitted to journal

**Subject Areas:**
paleontology, ecology, body size, migration, nursery

**Keywords:**
sand tiger, metapopulation, Eocene, Gulf of Mexico, Arctic, Antarctic, Delaware Bay, Carcharias taurus

**Author for correspondence:**
Sora Kim
e-mail: skim380@ucmerced.edu

# Supplementary Materials: Decoding the dynamics of dental distributions: insights from shark demography and dispersal

DOI:10.1098/rspb.2022.0808

Sora Kim[1,2,*], Justin D. Yeakel[1,*], Meghan Balk[3], Jaelyn J. Eberle[4], Sarah Zeichner[2,5], Dina Fieman[6], Jürgen Kriwet[7]

[1]School of Natural Science, University of California Merced,[2]Department of Geophysical Sciences, University of Chicago, [3]National Ecological Observatory Network, [4]Department of Geological Sciences and Museum of Natural History, University of Colorado, [5]Division of Geological and Planetary Sciences, California Institute of Technology, [6]School of Geography, Environment, and Earth Sciences, Victoria University of Wellington, [7]Department of Paleontology, University of Vienna *Contributed equally

THE ROYAL SOCIETY PUBLISHING

# Supplementary Appendix I. Geologic Settings and Taphonomy

## (a) Banks Island, NWT Canada

The fossil shark teeth were collected by JE and team over the course of three field seasons (2004, 2010, and 2012) from Eocene-aged strata near Muskox and Eames Rivers, within the boundaries of Aulavik National Park on northern Banks Island, NWT, Canada ( $74^{\circ}$N)[1]. The localities cannot be precisely correlated with one another, due to the distance between them and discontinuous exposures, although they contain the same shark taxa. Because the localities are within the boundaries of a national park, we are not able to provide more precise coordinates for the localities. Qualified researchers should contact the Canadian Museum of Nature (CMN) in Ottawa, ON, Canada, to request the exact coordinates.

The Eocene shark-bearing strata on Banks Island are assigned to the Cyclic Member of the Eureka Sound Formation [1–3]. The Cyclic Member comprises coarsening-upward cycles of shale, silt, unconsolidated sand, paleosol, and lignitic coal, and is interpreted as a deltaic sequence in a marginal marine setting [2]. Alongside thousands of shark teeth, scales and teeth of the bony fishes Atractosteus (gar), Amia (bowfin), and the percomorph teleost Eutrichiurides, as well as a vertebra of a crocodiliform [3], were recovered from the Cyclic Member. The unit also contains abundant bivalves and the trace fossil Ophiomorpha, interpreted as the burrow of a thalassinidean shrimp and generally indicative of shallow-water, moderately high energy, coastal marine environments [4]. Paleosalinity estimates that utilize the $\delta^{18}$O values of shark teeth indicate reduced surface salinity [5], which may explain why the shark fauna contains just four genera âĂŞ †*Striatolamia*, †*Carcharias*, †*Odontaspis*, and †*Physogaleus* [1].

The fossil shark teeth were recovered as float on unconsolidated sands in the Cyclic Member, a facies interpreted by Miall (1979) as distributary mouth bar deposits in the delta-front area. This was supplemented by dry screening to recover smaller specimens (i.e., small shark teeth). The Eocene age for the fossil localities near Muskox and Eames Rivers is based upon pollen samples initially analyzed by Hopkins [6,7] and reported by Miall (1979). Re-analysis of five pollen samples by Sweet [8] (discussed in [1]) suggests that the shark tooth localities near Muskox River are late early to middle Eocene in age and span the Early Eocene Climatic Optimum (EECO). Presence of †*Pistillipollenites* suggests a probable minimum age of middle Eocene for the samples, whereas the absence of †*Aquilapollenites tumanganicus* Bolotnikova and closely allied species, infrequent occurrences of †*Momipites* spp., and the richness of the angiosperm component of the assemblages precludes an earliest Eocene [1]. High resolution $\delta^{13}$C values from tree ring samples indicate a summer precipitation that was two to four times higher than in the winter [9]. An ocean paleotemperature of $12-13^{\circ}$C was estimated for the early-middle Eocene Arctic based on the TEX86 method [10]. A riverine temperature on Ellesmere Island was estimated to be around $9^{\circ}$C based on $\delta^{18}$O from terrestrial vertebrate bioapatite [11]. A crocodyliform fossil recovered from the Cyclic Member, as well as a tooth of the ray Myliobatis (a genus restricted today to tropical and warm temperate seas [1]) suggests a mild temperature on Banks Island in the early - middle Eocene.

## (b) Seymour Island, Antarctica

Seymour Island, Antartica The fossiliferous Eocene-?earliest Oligocene La Meseta Formation is part of Paleogene back-arc sediments that were deposited approximately 100 km SE of the northern tip of the Antarctic Peninsula representing the sedimentary filling of a generally northwest-southeast incised-valley system [12,13]. The 720 m massive sediments of the La Meseta Fm. overly unconformably either Late Cretaceous or Palaeocene deposits and originally were subdivided into seven lithofacies units named Telms 1-7 (Table 1). These lithofacies later were assigned to six erosionally-based internal units, named from base to top Valle de Las Focas, Acantilados, Campamento, Cucullaea I, Cucullaea II and Submeseta Allomembers [13], which

predominantly consists of poorly consolidated fine-grained sand- and mudstones interbedded with shell-rich conglomerates. These deposits were accumulated during the Eocene in deltaic, estuarine and shallow marine settings [13,14]. The coastal area was seemingly of low relief and comprises tidal channels and flats, an estuary mouth platform, as well as a mid-estuary [14,15]. Oxygen isotope ratio analysis of biogenic carbonate from bivalve fossils in La Meseta Fm. corroborate this cooling trend over the course of the Middle Eocene, estimating a temperature change from ca. $15^{\circ}$C (TELM 2) to ca. $10^{\circ}$C (TELM 5; [16,17]. Oxygen isotope ratio analysis of biogenic phosphate from sand tiger shark fossils in La Meseta Fm. suggest temperatures ranging from $12-13^{\circ}$C during the same time range, but do not see a similarly conclusive cooling trend [18]. Eocene terrestrial facies remain unknown from the Antarctic Peninsula indicating that the fossiliferous sites were deposited well off the coast and all terrestrial fossils were transported into the marine environment.

Detailed taphonomic studies of the fossil vertebrates remains still are very rare and mainly have focused on fossil penguin elements up to now [19,20]. Nevertheless, the environmental settings of the fossiliferous sites (Table 1) and the corresponding dynamic systems might have had an influence on fossil preservation and probably also had some sorting effects. Teeth of †*Straitolamia macrota* were recovered from all TELMS in various quantities (Tab. 1) and preservational conditions. While most of older fossil collections only include larger, surface collected shark teeth, more recent collections also contain smaller shark and ray teeth that were obtained from bulk sediment samples that were sieved and subsequently sorted under a microscope. The high abundance of small-toothed taxa (e.g., batomorphs, carcharhiniforms) as well as small teeth of taxa that previously were represented almost exclusively by large teeth (e.g., lamniforms) in TELMs 3-5 imply that at least in these units a collecting bias can be ignored. The various preservational states ranging from complete conservation of small and large teeth to isolated tooth crowns of mainly large teeth indicate that different taphonomic events were at work. The high number of isolated tooth crowns of large teeth suggests that these teeth might have been exposed on the surface for longer times. The presence of small teeth most likely representing juveniles and larger teeth of subadults and adults, however, demonstrate that the collections used in this study most likely were not heavily plagued by collecting biases. Conversely, †*S. macrota* is represented by rare large teeth in Telms 1, 2, 6 and 7 suggesting either collecting bias (targeting larger teeth during surface collecting) or sorting effects in these units. Detailed collection effort and taphonomic analyses will help to better understand the various biotic and abiotic effects on shark, ray, and skate tooth preservation modes throughout the Eocene La Meseta Fm. in the future.

## (c) Red Hot Truck Stop, Meridian, Mississippi

†*Striatolamia macrota* teeth used in this study were collected from the Red Hot Truck Stop locality by K.C. Beard and a Carnegie Museum of Natural History (CM) team in 1990 âĂŞ 1994 and 2000 near Meridian, Mississippi. The fossil locality, also known as CM locality 517, occurs in the uppermost Tuscahoma Formation, interpreted as earliest Eocene (early Wasatchian) in age on the basis of the mammalian fauna [21], palynology [22], and radiometric (K-Ar) ages [23].

The vertebrate fossils from CM locality 517 are concentrated along with plant debris and rip-up clasts of mudstone in a channel lag at the base of the T4 sand, the uppermost sedimentary unit in the Tuscahoma Formation [24]. The T4 sand at the Red Hot Truck Stop locality ranges in thickness from just a few cm to more than a meter, is green in color, and comprised of unconsolidated fine- to very fine-grained quartz sand, glauconite, and mica [25]. Based on both the lithology and the vertebrate fauna, the T4 sand is interpreted as estuarine channel facies deposited at a time when sea level along the Gulf Coastal Plain was high [23–25]. The vertebrate faunal assemblage from the T4 sand includes over 30 species of selachians and 11 species of bony fishes [26–28] as well as snakes [29], birds, lizards, crocodilians, and nine orders of mammals [21,24,30]. The diverse pollen floras indicate a paratropical biome [22]. Ten shells were analyzed and resulted in a MAT (Mean Annual Temperature) of $26.5 \pm 1.0^{\circ}$C; $2-3^{\circ}$C warmer than modern sea-surface MAT in

the northern Gulf of Mexico [31]. Analysis of mollusk shells from the Gulf Coast by Kobashi et al. [32] found that the climate of the Mississippi Embayment (paleolatitude of $30^{\circ}$N) changed from a tropical environment of $26-27^{\circ}$C in the Eocene, to paratropical, $22-23^{\circ}$C in the Oligocene Epoch. Using modern regional salinity of 33 ppt, and the equation sought out by Grossman and Ku [33], the estimated MAT of the Eocene Gulf Coast ocean water was approximately $23.3 \pm 5^{\circ}$C, slightly cooler than the continental temperature [32].

The vertebrate fossils were recovered by screen-washing the fossiliferous parts of the T4 sand (Beard, pers. comm. to JE, 2022). Beard and Dawson [21] noted that the mammalian component of CM locality 517 differs from early Wasatchian assemblages in the U.S. Western Interior in its abundance of smaller-bodied species and underrepresentation of medium to large-bodied species of mammal. These authors hypothesized that this may reflect size-sorting in the estuarine channel environment and the use of screen-washing to recover the fossils, whereas faunas recovered primarily through surface collection are known to underestimate the abundance of small mammals [34,35].

## (d) Whiskey Bridge, Burleston County, TX USA

The Whiskey Bridge locality is part of the Stone City Member, which lies within the late Middle Eocene Crockett Formation, overlying the Sparta Sand Formation and as part of the larger late Middle Eocene Claiborne Group [36–39]. The Member is made up of a variety of bedforms that expose a thick transgressive sequence [39]; strata preserve both marine, nearshore features, with preservations of bioclasts, burrows, and vertebrate fossils [39–41], along with intervals of terrestrial river water inputs. This near-shore marine interpretation is supported by X-ray Diffraction and Mossbauer spectral analyses of clay pellets from the Stone City Member, which suggest normal marine conditions and basic pH (7.5-8.5) [39].

The Stone City Member has undergone minimal taphonomic alteration, and preserves one of the most diverse Middle Eocene vertebrate fauna within the Gulf Coastal Plain [40]. These diverse taxa include shallow neritic dwellers (i.e., gastropods, bivalves, ootolith-based taxa, rays, teleost fish, reptiles and sharks) and low to moderate diversity of foraminifera [36,40]. The extant fauna is comparable to modern Gulf Coastal Plain fauna living in shallow inner shelf marine waters, and suggests that Stone City Fm. preserves a record of a tropical to sub-tropical climate with normal marine salinity [36,38,39]. Specifically, Stone City Member preserves three species of sand tigers (*Carcharias cuspidata*, *C. hopei*, *Striatolamia macrota* [36]). The extant fauna is comparable to modern Gulf Coastal Plain fauna living in shallow inner shelf marine waters, and suggests that Stone City preserves a record of a tropical to sub-tropical climate with normal marine salinity [36,38,40].

Broadly, the sedimentology of the Stone City Member preserves three distinct depositional modes: primary shelf sediments dominated by dark glauconitic clay-silts and a matrix supported fossil assemblage that suggest marine near shore deposition, large deposits of fossils and bioclasts which suggest high energy storm deposition, and fine sandstone deposit with preserved burrows which represent a low energy marine environment [41]. The high energy storm environment is useful for deposition of large vertebrate fossils [39](personal communication to SSZ, 2022). Shark teeth are sampled from the PQ sands within the Stone City Member, which is a unit of unlaminated upward fining sandstone [36–39] (personal communication to SSZ, 2022). The fauna collected from the PQ sands included 14 species of shark, 11 species of fish, 12 species of rays/batoids, 5 species of reptiles and 1 specimen of mammal, as well as teredolites, wood logs, octocorals and otoliths. The majority of the shark teeth were collected from the base of the unit, over many years (personal communication to SSZ, 2022). It is possible that the high energy storm system could have preferentially deposited larger clasts. However, our wide distribution of tooth heights from the MGB suggests that both small and larger teeth were well preserved. This is also supported by the range of fossils present from both marine and terrestrial environments.

### (e) Analysis of sample size and moment estimation

Because some dental distributions are distinctly non-Normal, we assessed the effect of sample size using a simulation approach. For each locality, we initiated sampling schemes varying from $n = 10$ to $500$ samples, and calculated various shape parameters averaged across $1000$ replications. As also shown with a standard parametric power analysis, the lower-order moments (mean, standard deviation) and medians require very few samples for accurate estimation. Parametric tests reveal that estimation of lower moments to within a 10% accuracy requires samples on the order of $n = 24$ (Banks Island) $n = 41$ (Seymour Island), $n = 35$ (Red Hot Truck Stop), and $n = 16$ (Whiskey Bridge). While some of these distributions violate normality, a non-parametric assessment of sampling accuracy confirms that roughly 50 samples enable estimation accuracy of at least $0.5$ mm across all sites, with some sites requiring far fewer for a similar degree of accuracy (Supplementary Figure 1). In all cases, our sampling effort at each locality allows for an estimation accuracy of these lower-order parameters within 0.2-0.5 mm. We also show with our non-parametric approach that while 25th and 75th percentiles require similar sample sizes for accurate estimation in most cases (the 75th percentile is not as well estimated for Seymour Island), estimation of major (highest) and/or minor (second-highest) modes are always less accurate. This is expected because modes are higher-order features of distributions, and can sometimes be subtle, which can require large sample sizes to detect. Regardless, we observe that in all cases our sampling effort allows for estimation accuracy of the major mode to be within 1-2 mm.

## Supplementary Appendix II. Population simulation

To explore specific ecological mechanisms that may be responsible for the observed dental distributions, we employed a process-based model allowing us to incorporate likely physiological and ecological constraints influencing shark populations. We constructed a two-site size-class model that tracks female shark populations over time, where one of the two sites is designated a juvenile site, or nursery, and the other is designated an adult site (main text figure 2). Because there is dispersal from the juvenile to adult site, and from the adult to juvenile site, each locality hosts a complex size-structure formed from a mixture of younger and older shark individuals, and it is this mixture from which accumulated tooth distributions are derived.

We considered four key dynamics influencing changes in population size for both sites: reproduction, somatic growth, mortality, and dispersal between sites. We set juvenile/adult sites to be 700 Km [42,43] and 400 Km apart for Eocene sites, where seasonal fluctuations in temperature reached site-specific minimum (winter) and maximum (summer) extremes, allowing us to consider the effects of locations farther from and closer to the equator (temperature parameters are reported in the Results and Discussion). By simulating shark population dynamics we tracked changes in population size structure as reflected by teeth, which are strongly correlated with size [44]. A comparison of simulated body size distributions against those observed from different environments thus allows us to propose specific ecological mechanisms giving rise to observed features in empirical size structure, and the resulting accumulated dental distributions, from site to site. Because there is not significant sexual dimorphism among sand tigers [45], our model considers only the population dynamics of females.

In our framework, reproduction takes place only at the juvenile site, whereas mortality occurs at both sites. The per-capita reproductive rate $r$ was thus set to $r = 0$ at the adult site, and $r = 0.47 \times 10^{-7}$ female inds/s [46] at the juvenile site, independent from time of year or water temperature. The per-capita mortality rate was assumed to be constant across size classes within both juvenile and adult sites at $\mu = 5.71 \times 10^{-9}$ inds/s [47]. Shark individuals were assumed to increase in mass $m$ (g) following the growth trajectory described by West et al. [48] as a function of metabolic rate. Metabolism $B$ (W·g$^{-3/4}$, where W is watts) is partitioned between somatic growth and maintenance, providing a general equation for ontogenetic growth trajectories [48]. Ontogenetic growth is derived from the balance condition $B_0(T)m^{\eta} = E_m\dot{m} + B_m(T)m$ , where $E_m = 5774$ (J/g) is the energy needed to synthesize a unit of mass [49], $B_m(T)$ is the temperature

(T)-dependent metabolic rate to support an existing unit of mass, $B_0(T)$ is the temperature-dependent metabolic normalization constant, and temperature is in Kelvin [48]. The time that it takes to reach size $m$ as an individual grows from the initial mass $m_0$ to the asymptotic adult mass $M$ is given by the timescale

$$\tau\left(m\right) = \ln\left[\frac{1-\left(m_0/M\right)^{1-\eta}}{1-\left(m/M\right)^{1-\eta}}\right]\frac{M^{1-\eta}}{\alpha(T)\left(1-\eta\right)}, \tag{S1}$$

given $\alpha(T) = B_0(T)/E_m$, and the scaling exponent $\eta = 3/4$ [50]. Because contemporary and Eocene sand tigers are assumed to be ectotherms, we incorporate a temperature-dependence for metabolic parameters, such that $B_0(T) = \exp[C - E/kT]$, where the normalization constant $C = 18.47$ for fish, the activation energy $E = 0.63$ (eV; electron volts), and Boltzmann's constant $k = 8.6173 \times 10^{-5}$ (eV/Kelvin) [51]. Accordingly, shark individuals grow more quickly in warm environments, reaching the asymptotic mass $M$ at a younger age. We assume each site varies in temperature along a sinusoidal trajectory, from a summer maximum to a winter minimum and back over the course of a year, such that individuals in both juvenile and adult sites experience local seasonal variation in temperature as they migrate from site to site.

In our two-site model, juveniles disperse to the adult site once they have reached a particular mass, and adult females migrate annually from the adult to juvenile site to reproduce. The maximal migration rate is assumed to be a function of the distance between the nursery and the adult site, such that $d_{\max} = v/\delta$, where velocity $v = 1$ (m/s) and $\delta$ (m) is distance. The initial dispersal of juveniles to the adult site and annual dispersal of adults to the juvenile site are considered separately because we assume these events are mass-dependent and time-dependent, respectively. When newborns of size $m_0$ are born in the juvenile site, we assume they begin dispersing to the adult site at the threshold mass of $m_j = (1/4)M$ (g).

A strict juvenile dispersal strategy means that initial dispersal to the juvenile site occurs when individuals reach $m_j$. A flexible juvenile dispersal strategy means that dispersal may occur at sizes smaller or larger than $m_j$. If the initial dispersal rate of juveniles to the adult site $d_{j\to a}^{\text{initial}}(m)$ is mass-dependent, varying from $d = 0$ near $m_0$ and increasing sigmoidally to $d = d_j^{\max}$ above $m_j$, it can be described as

$$d_{j\to a}^{\text{initial}}(m) = \frac{d_j^{\max}}{1+\exp\left[\frac{-(m-m_j)}{\xi_j}\right]}, \tag{S2}$$

where $\xi_j$ describes the flexibility of the size-dependent migration. In other words, as juveniles increase in size to $m_j$, their migration rate to the adult site increases sigmoidally to $d_{\max}$. Adults occupying the juvenile site disperse back to the adult site at a constant rate, having already attained $d_{\max}$. The juvenile dispersal window $\xi_j$ describes the flexibility of this mass threshold: a smaller dispersal window (low $\xi_j$) means that initial dispersal of juveniles to the adult site operates around a strict mass threshold $m_j$, whereas a large juvenile dispersal window (high $\xi_j$) means that initial dispersal of juveniles to the adult site is flexible around $m_j$. Importantly, a low juvenile dispersal window also implies that the juvenile site is serving a separate function than the adult site - in other words, the juvenile site is operating as a distinct nursery where juveniles must reside until a particular threshold size.

We assume that individuals occupying the adult site disperse back to the juvenile site to reproduce annually, such that the adult dispersal rate $d_{a\to j}^{\text{annual}}(t)$ is a function of time. Accordingly, the dispersal rate is maximized to $d_a^{\max}$ on a particular day each year $t_{\text{peak}}$, and decreases to zero in a Gaussian manner before and after. Annual adult dispersal from the adult site to the juvenile site is thus described as

$$d_{a\to j}^{\text{annual}}(t) = d_a^{\max}\exp\left[\frac{-(t-t_{\text{peak}})^2}{2\xi_a^2}\right]. \tag{S3}$$

The adult dispersal window $\xi_a$ describes the flexibility of this annual dispersal: a smaller dispersal window (low $\xi_a$) means that annual adult dispersal to the juvenile site operates around a strict peak day, whereas a large adult dispersal window (high $\xi_a$) means that annual adult dispersal to

the juvenile site is flexible. We note that the resolution and range of juvenile and adult dispersal windows had to be adjusted from site to site to account for simulation limitations related to population dynamics in different temperature environments.

Because we aim to understand the shapes of dental distributions from the perspective of shark population dynamics, we must simulate the loss and accumulation of teeth over time in both juvenile and adult sites. We focus only on the loss of the first upper and lower anterior teeth (A1 and a1) to reflect those used to build the empirical distributions. To simulate accumulated dental distributions, we assumed a similar rate to *Triakis semifasciata* with a tooth loss rate of one upper and lower tooth every 40 days [52]; although this species differs from sand tigers, it is the only species with an experimentally controlled, quantitative measurement of tooth drop. This rate of tooth drop corresponds to $5.79 \times 10^{-7}$ teeth/s. Inclusion of tooth drop rate seasonality has little impact on model results (Supplementary Figure 2-3).

## Supplementary Appendix III. Settings for contemporary and Eocene sand tiger populations

To capture conditions representative of the migratory environment experienced by sand tigers along the Massachusetts to Delaware coastline, we set the minimum and maximum temperatures of the simulated juvenile site to $17^{\circ}$C and $25^{\circ}$C, and the minimum and maximum temperatures of the simulated adult site to $13^{\circ}$C and $23^{\circ}$C [42,43,53], where we assumed a distance of 700 Km separating sites.

High latitude locations include the Banks Island (Canada) brackish and Seymour Island (Antarctic) marine sites, whereas low latitude locations include the Red Hot Truck Stop (MS) estuary and Whiskey Creek (TX) marine sites. Reconstruction of temperature regimes vary from high- to low-latitude sites. High-latitude sites have more extreme summer highs and winter lows with exaggerated differences between coastal and pelagic environments, with brackish (juvenile site) habitats ranging from $12^{\circ}$C to $24^{\circ}$C [10,54] and marine (adult site) habitats ranging from $9^{\circ}$C to $17^{\circ}$C [18,54–56]. In contrast, low-latitude sites have more equitable summer highs and winter lows with less extreme differences between coastal and pelagic environments, with both brackish and marine habitats ranging from $23^{\circ}$C to $30^{\circ}$C [31]. For all Eocene localities, we set the distance between juvenile and adult sites to 400 Km. While we do not know the actual distances separating juvenile and adult sites in the Eocene, even large differences in distance have negligible effects on tooth distributions (e.g. $\pm 150$ Km differences in distance result in $< 1\%$ change in distributional means; Supplementary figure 4).

## Supplementary Appendix IV. Dispersal drives diverse dental distributions

The results of our population simulation reveal that changes in the initial dispersal of younger sharks from the juvenile site to the adult site, and of older sharks from the adult to juvenile site, can drastically change the shape of dental distributions within both sites (main text figure 3). Specifically, we examine the effects of increasing flexibility in the onset of these different dispersal events, where the initial migration of younger sharks to the adult site is a function of their mass ($\xi_j$; x-axis in main text figure 3) and adult migration to the juvenile site is a function of the time of year ($\xi_a$; y-axis in main text figure 3). We distinguish four quadrants capturing the range of variation in dental distribution geometries that result from different juvenile and adult dispersal strategies in main text figure 3 (regions I-IV). We emphasize that our simulation framework is designed to examine whether the dispersal strategies described are able to account for the variation observed among empirical dental distributions, in part due to the limited ecological information we have for extinct taxa from the fossil record. We cannot discount alternative influences such as those stemming from the effects of intra- and inter-specific competition, higher-trophic species interactions, or evolutionary drivers, which we do not examine here. Results

of all contemporary and Eocene sites exhibit the same qualitative features, so we focus on high-latitude Eocene sites, for which we were able to maximize resolution (main text figure 3). Results for the contemporary Delaware population and the low-latitude Eocene sites are shown in Supplementary Figures 5-6.

As dispersal windows increase, both the initial dispersal of juveniles to the adult site and the annual dispersal of adults to the juvenile site varies widely. For a shark with an asymptotic mass of 350 kg, where we assume maturity is reached at $m_j = 87$ kg, the initial migration to the adult site ranged from 0.5 kg around $m_j$ (low flexibility) to 87 kg around $m_j$, effectively meaning it can migrate at any time after birth (high flexibility). In contrast, adult dispersal back to the juvenile site is a function of time, and we allowed this dispersal window to vary from 1 day around the peak dispersal day (low flexibility) to up to 50 days around the peak dispersal day (high flexibility). With maximum flexibility in both juvenile and adult dispersal windows (high $\xi_j$ and $\xi_a$), we observe the fallen teeth accumulating at each site to converge towards a single distributional geometry at both sites (region II in main text figure 3), an effect of highly mixed juvenile and adult populations. As both dispersal windows decrease towards minimal flexiblity (low $\xi_j$ and $\xi_a$), we observe the dental distributions to become distinct, with a very low and very high mean tooth size in the juvenile and adult site, respectively (region III in main text figure 3), an effect of strict size-based and temporal dispersal constraints.

When initial juvenile and annual adult dispersal windows are asymmetric, the shapes of accumulated dental distributions at each site become less intuitive. If the size at which juveniles first disperse to the adult site is strict (small $\xi_j$) and the timing of adult migration varies widely (large $\xi_a$), we observe that *i*) the mean of the juvenile distribution is much lower than the mean of the adult distribution, and *ii*) the variance of the juvenile distribution is large while the variance of the adult distribution is small (region I, main text figure 3). Because juvenile dispersal is restricted, they cannot travel to the adult site until they reach $m_j$, lowering the representation of smaller size classes in the adult site. However, because adult dispersal is more flexible, there is increasing representation of adult size-classes in the juvenile site, increasing variability.

If the size at which juveniles first disperse to the adult site is variable (large $\xi_j$) and the timing of the adult migration is strict (small $\xi_a$), we observe *i*) the emergence of two distinct modes in the dental distributions accumulating at both sites, and *ii*) asymmetry in modal frequencies at the juvenile site where the smaller mode is emphasized, and more even modal frequencies at the adult site (region IV in main text figure 3). Bimodality in dental distributions generally occurs when adult dispersal is restricted ($\xi_a < 30$ days) but across a relatively large range of juvenile dispersal mass ($\xi_j > 50$ kg). Accordingly, the initial dispersal of juveniles is independent of size, while annual adult dispersal is more restricted.

There are two forces acting to promote bimodality. First, increased variability in juvenile body size initiating dispersal to the adult site results in greater representation of smaller size-classes at the adult site. Second, lower dispersal flexibility at the adult site means that individuals have a chance to grow in body size before they return to the juvenile site to reproduce, increasing differences in size-classes between the two sites. The frequency asymmetry at the juvenile site is largely due to an over-representation of offspring prior to initial dispersal.

Juvenile sharks may leave their natal site – often in shallow estuaries [42,57] – to less protected pelagic environments across a range of sizes and times, depending on the availability of resources and predation pressure [58]. Importantly, a juvenile site functions as a nursery if and only if there is a size threshold governing an individual's initial migration to the adult site. If migration out of the nursery is fluid and independent of size, the site is assumed to no longer provide a size-dependent fitness advantage, such that a designation of 'nursery' is unmerited. We observe that variation in the onset of these dispersal events – the initial dispersal of juveniles to a pelagic adult site, and annual returns of adults to a juvenile site to reproduce – has profound effects on the shapes of shark tooth distributions accumulating at both sites. Having established this range of ecological drivers on distribution shape, we next examine whether and to what extent we

can extract ecological meaning from the shape of an extant sand tiger size distribution, and then extend our approach to interpret the dental distributions from Eocene deposits.

## Supplementary Appendix V. Supplemental Tables

| Site | Banks Island | Seymour Island | Red Hot Truck Stop | Whiskey Bridge | Delaware Bay |
|---|---|---|---|---|---|
| Formation | Eureka Sound | La Meseta | Bashi/Tuscahoma | Crockett | modern |
| Latitude | 73°43′N | 64°17′S | 32°38′N | 30°63′N | 38°52′N |
| Longitude | 120°46-51′W | 56°45′W | 88°65′W | 96°54′W | 75°2′W |
| Habitat | Brackish | Marine | Brackish | Marine | mix |
| N ATCH | 397 | 126 | 372 | 158 | 137 |
| D′Angostino Test | | | | | |
| skew | -0.1084 | 0.8009 | 0.4725 | 0.1368 | 0.5231 |
| z | -0.8953 | 6.3373 | 3.1796 | 0.7289 | 2.480 |
| p-value | 0.37 | « 0.0001 | 0.0015 | 0.47 | 0.013 |
| Kurtosis - Bonett Test | | | | | |
| tau | 2.9512 | 5.2225 | 3.0971 | 3.8681 | 2.0870 |
| z | -6.2215 | 0.7680 | -1.1280 | -2.7321 | 2.6309 |
| p-value | «0.0001 | 0.44 | 0.26 | 0.0063 | 0.0085 |
| skew | -0.1084025 | 0.8009457 | 0.4724565 | 0.1367579 | 0.5230945 |
| kurtosis | 1.927971 | 3.328463 | 2.845512 | 2.168379 | 3.273326 |
| moment | 13.70411 | 19.21683 | 12.62215 | 22.50671 | 18.91735 |

Supplementary Table 1: stuff

# Supplementary Appendix VI. Supplemental Figures

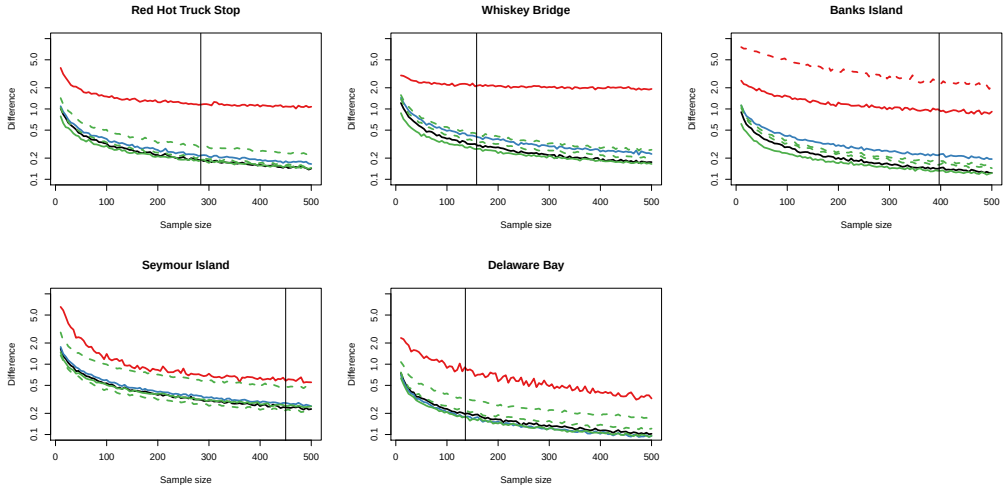


Supplementary Figure 1: Simulation results that show the effect of sample size on the estimation accuracy of different dental distribution shape parameters across both contemporary and Eocene localities. Difference is measured as $\sqrt{(\text{obs} - \text{sim})^2}$ where obs is the empirical value and sim is the simulated value for a given sample size. Black solid line = mean; blue solid line = median; green solid line = standard deviation; green dashed lines = 25th and 75th percentiles; red solid line = major (highest) mode; red dashed line = minor (second-highest) mode if it is detected.

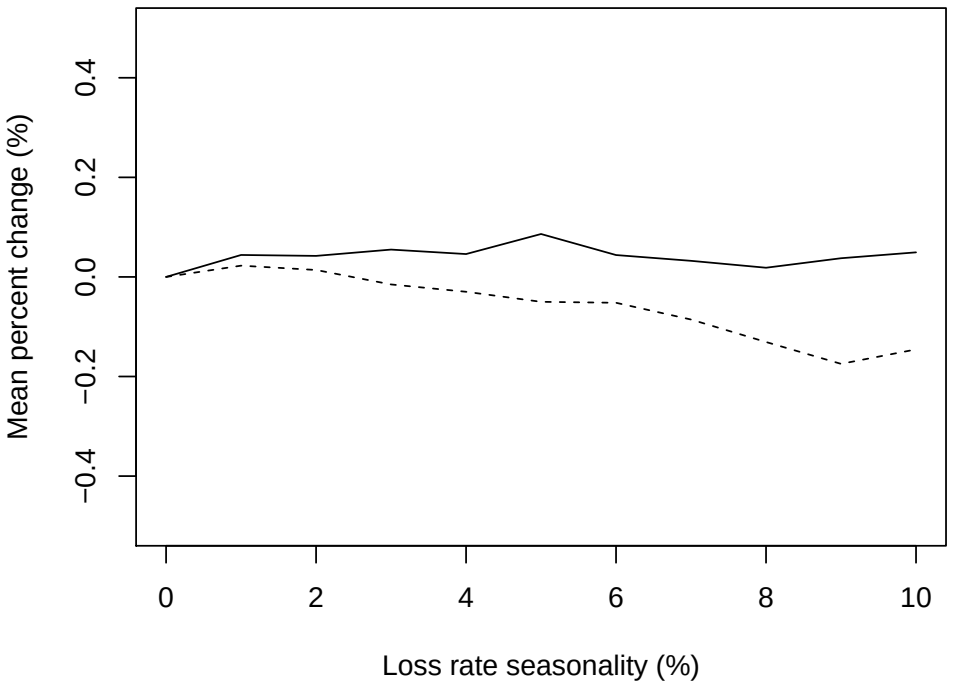


Supplementary Figure 2: Mean percent change of model results as a function of tooth drop rate seasonality, where maximum drop rates occur during the peak of the cold season. Mean percent change (%) is calculated as the percent change in simulated tooth distribution means averaged across juvenile and adult dispersal window values. Increasing shedding rate seasonality refers to an $X\%$ increase in shedding rate during the cold season, followed by an $X\%$ decrease during the warm season. Dashed lines denotes changes in juvenile site distribution means, whereas solid lines denote changes in adult site distribution means. An increase/decrease in tooth drop rate of 10% during the cold/warm season resulted in a ca. 0.2% decrease in juvenile site means, and no change in adult site means.

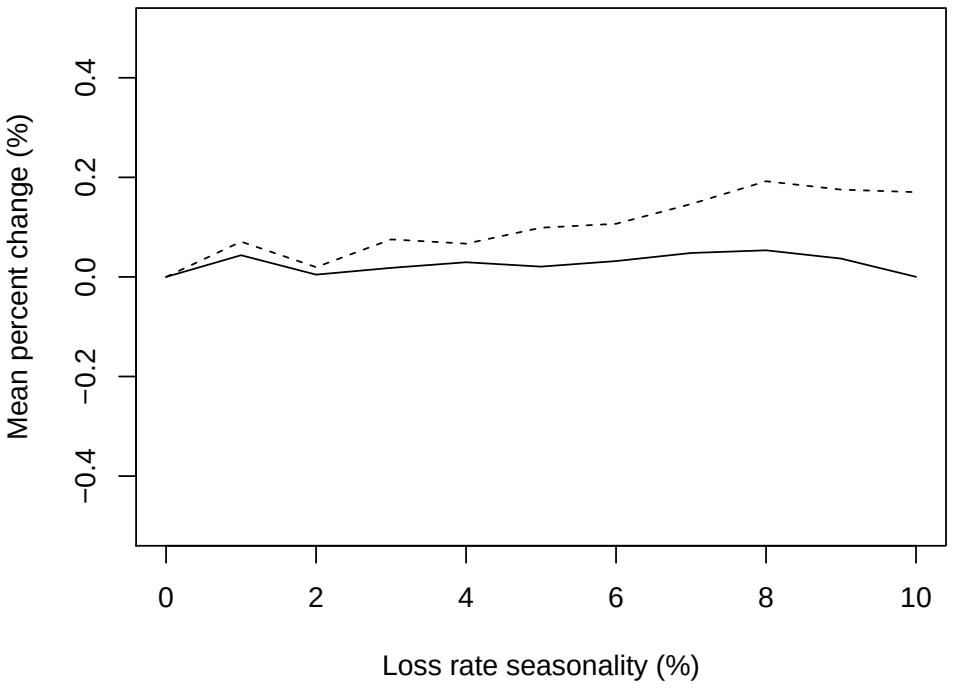


Supplementary Figure 3: Mean percent change of model results as a function of tooth shedding rate seasonality, where maximum shedding rates occur during the peak of the warm season. Mean percent change (%) is calculated as the percent change in simulated tooth distribution means averaged across juvenile and adult dispersal window values. Increasing shedding rate seasonality refers to an $X\%$ increase in shedding rate during the warm season, followed by an $X\%$ decrease during the cold season. Dashed lines denotes changes in juvenile site distribution means, whereas solid lines denote changes in adult site distribution means. An increase/decrease in tooth drop rate of 10% during the warm/cold season resulted in a ca. 0.2% increase in juvenile site means, and no change in adult site means.

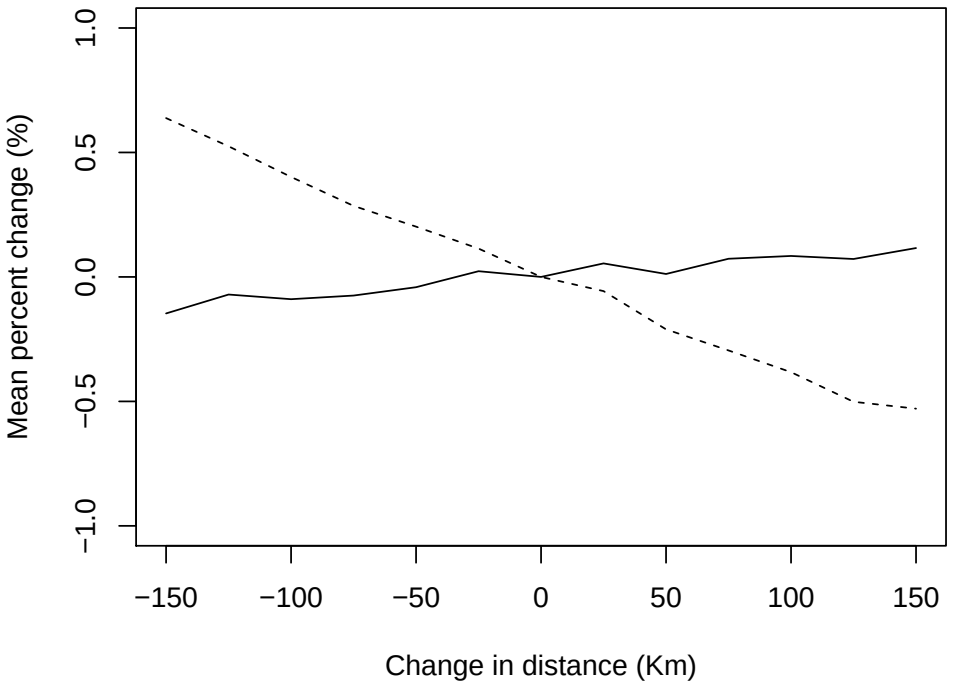


Supplementary Figure 4: The effect of decreasing and increasing distance on simulated dental distribution means, averaged across $\xi_j$ and $\xi_a$, for contemporary sand tiger populations. Changes in the juvenile site distributions are denoted by the dashed line; changes in the adult site distributions are denoted by the solid line. In all cases, decreasing or increasing distance $\pm 150Km$ results in a mean percent difference in distributional means of $< 1\%$.

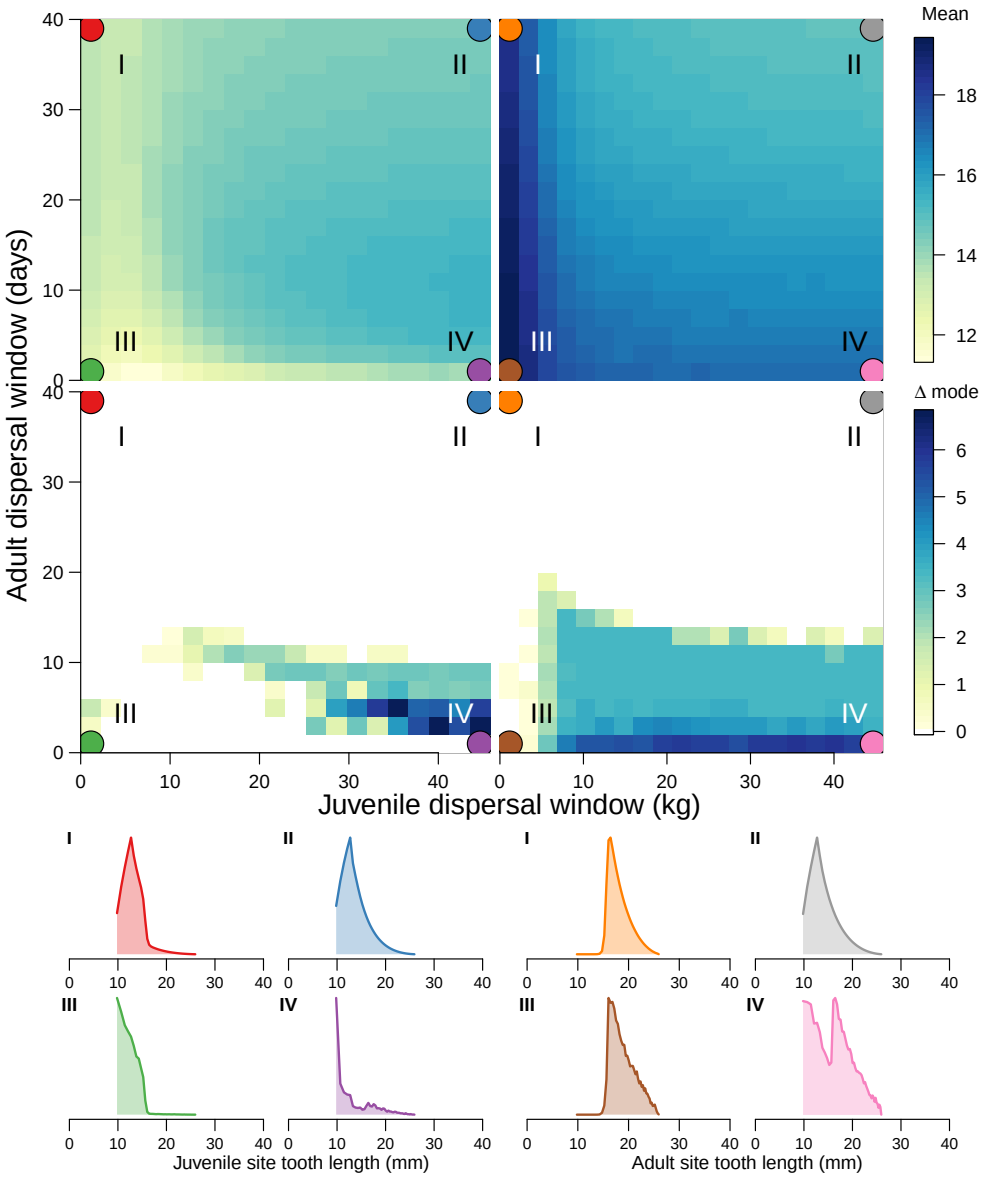


Supplementary Figure 5: Simulation results for the dynamic population model as a function of juvenile and adult dispersal windows ($\xi_j$ and $\xi_a$, respectively) given conditions experienced by the contemporary Delaware Bay population. Changes in dental distribution shape are captured by site-specific means (top two panels) and the distance between modes ($\Delta$ mode; bottom two panels). A $\Delta$ mode value of zero means there is only one mode. Representative distributions of anterior tooth crown height are shown for juvenile site and adult sites for regions I-IV (horizontal along bottom and vertical along right edge, respectively), where color denotes both region and site identity. Regions I-IV depict various combinations of small and large dispersal windows. Region I (high $\xi_a$, low $\xi_j$); II (high $\xi_a$, high $\xi_j$); III (low $\xi_a$, low $\xi_j$); IV (low $\xi_a$, high $\xi_j$).

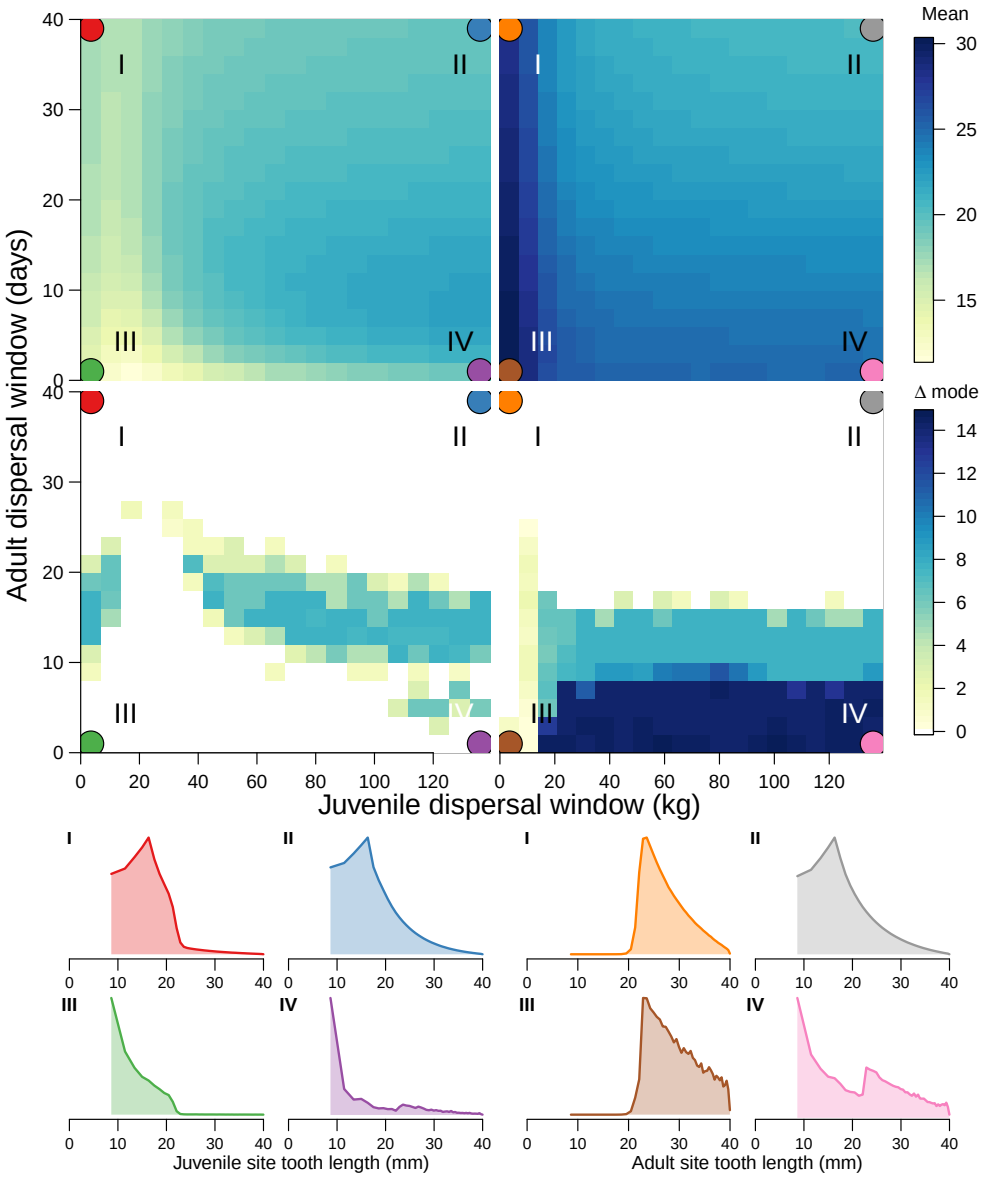


Supplementary Figure 6: Simulation results for the dynamic population model as a function of juvenile and adult dispersal windows ($\xi_j$ and $\xi_a$, respectively) given low latitude Eocene conditions. Changes in dental distribution shape are captured by site-specific means (top two panels) and the distance between modes ($\Delta$ mode; bottom two panels). A $\Delta$ mode value of zero means there is only one mode. Representative distributions of anterior tooth crown height are shown for juvenile site and adult sites for regions I-IV (horizontal along bottom and vertical along right edge, respectively), where color denotes both region and site identity. Regions I-IV depict various combinations of small and large dispersal windows. Region I (high $\xi_a$, low $\xi_j$); II (high $\xi_a$, high $\xi_j$); III (low $\xi_a$, low $\xi_j$); IV (low $\xi_a$, high $\xi_j$).

## References


1. Padilla A, Eberle JJ, Gottfried MD, Sweet AR, Hutchison JH. 2014 A sand tiger shark-dominated fauna from the Eocene Arctic greenhouse. *Journal of Vertebrate Paleontology* **34**, 1307–1316.
2. Miall AD. 1979 Mesozoic and Tertiary geology of Banks Island, Arctic Canada: the history of an unstable craton margin. *Geological Survey of Canada Memoir* **387**, 1–235.
3. Eberle JJ, Gottfried MD, Hutchison JH, Brochu CA. 2014 First record of Eocene bony fishes and crocodyliforms from CanadaâĂŹs Western Arctic. *PloS one* **9**, e96079.
4. Frey RW, Howard JD, Pryor WA. 1978 Ophiomorpha: its morphologic, taxonomic, and environmental significance. *Palaeogeography, Palaeoclimatology, Palaeoecology* **23**, 199–229.
5. Kim S, Eberle J, Bell D, Fox D, Padilla A. 2014 Evidence from shark teeth for a brackish Arctic Ocean in the Eocene greenhouse. *Geology* **42**, 695–698.
6. Hopkins W. 1974 Report on 36 Field Samples from Banks Island, District of Franklin, Northwest Territories, Submitted by A. Miall, 1973 (NTS 88C, F, 98D, E), Geological Survey of Canada. Technical report Paleontological Report KT-01-WSH-1974.
7. Hopkins W. 1975 Palynology Report on 44 Field Samples from Banks Island, Submitted by AD Miall, 1974 (NTS 88B, C, F, 97H, 98D, E); Geological Survey of Canada. Technical report Paleontological Report KT-10-WSH-1975.
8. Sweet A. 2012 Applied research report on 5 outcrop samples collected by Andrew Miall from northern Banks Island. *NWT (NTS Map Sheets 098E/01, 08, 09): Geological Survey of Canada Paleontological report ARS-2012-01*.
9. Schubert BA, Jahren AH, Eberle JJ, Sternberg LS, Eberth DA. 2012 A summertime rainy season in the Arctic forests of the Eocene. *Geology* **40**, 523–526.
10. Sluijs A, Röhl U, Schouten S, Brumsack HJ, Sangiorgi F, Damsté JSS, Brinkhuis H. 2008 Arctic late Paleocene–early Eocene paleoenvironments with special emphasis on the Paleocene-Eocene thermal maximum (Lomonosov Ridge, Integrated Ocean Drilling Program Expedition 302). *Paleoceanography* **23**.
11. Eberle JJ, Fricke HC, Humphrey JD, Hackett L, Newbrey MG, Hutchison JH. 2010 Seasonal variability in Arctic temperatures during early Eocene time. *Earth and Planetary Science Letters* **296**, 481–486.
12. Del Valle R, Elliot D, Macdonald D. 1992 Sedimentary basins on the east flank of the Antarctic Peninsula: proposed nomenclature. *Antarctic Science* **4**, 477–478.
13. Marenssi SA. 1998 *Paleoambientes sedimentarios de la Aloformación La Meseta (Eoceno), Isla Marambio (Seymour), Antártida*. Number 464. Dirección Nacional del Antártico, Instituto Antártico Argentino.
14. Marenssi SA, Santillana SN, Rinaldi CA. 1998 Stratigraphy of the La Meseta Formation (Eocene), Marambio (Seymour) Island, Antarctica. *Publicación Electrónica de la Asociación Paleontológica Argentina* **5**.
15. Marenssi S. 1995 Sedimentología y paleoambientes de sedimentació de la Formación La Meseta, isla Marambio, Antártida, Parts I ér II. PhD thesis (unpublished).. .
16. Dutton AL, Lohmann KC, Zinsmeister WJ. 2002 Stable isotope and minor element proxies for Eocene climate of Seymour Island, Antarctica. *Paleoceanography* **17**, 6–1.
17. Ivany LC, Lohmann KC, Hasiuk F, Blake DB, Glass A, Aronson RB, Moody RM. 2008 Eocene climate record of a high southern latitude continental shelf: Seymour Island, Antarctica. *Bulletin of the Geological Society of America* **120**, 659–678.
18. Kim SL, Zeichner SS, Colman AS, Scher HD, Kriwet J, Mörs T, Huber M. 2020 Probing the ecology and climate of the Eocene Southern Ocean with sand tiger sharks Striatolamia macrota . *Paleoceanography and Paleoclimatology* pp. 1–21.
19. García R, Acosta Hospitaleche C, Márquez G. 2021 Biodeterioration of Antarctic fossil penguin bones caused by lichens from the Eocene La Meseta Formation. *Polar Biology* **44**, 2243–2254.
20. Irazoqui F, Acosta Hospitaleche C. 2021 Bioerosive traces in fossil penguin bones (Aves, Sphenisciformes) from the Eocene of Marambio/Seymour Island (West Antarctica). *Historical Biology* pp. 1–9.

21. Beard KC, Dawson MR. 2001 Early Wasatchian mammals from the Gulf Coastal Plain of Mississippi: Biostratigraphic and paleobiogeographic implications. In *Eocene Biodiversity* , pp. 75–94. Springer.
22. Harrington GJ. 2003 Wasatchian (Early Eocene) pollen floras from the Red Hot Truck Stop, Mississippi, USA. *Palaeontology* **46**, 725–738.
23. Mancini EA, Tew BH. 1995 Geochronology, Biostratigraphy and Sequence Stratigraphy of a Marginal Marine to Marine Shelf Stratigraphic Succession: Upper Paleocene and Lower Eocene, Wilcox Group, Easter Gulf Coastal Plane, USA. .
24. Beard KC, Dawson MR. 2009 Early Wasatchian mammals of the red hot local fauna, uppermost Tuscahoma formation, Lauderdale County, Mississippi. *Annals of Carnegie Museum* **78**, 193–243.
25. Ingram S. 1991 The Tuscahoma-Bashi section at Meridian, Mississippi: First notice of lowstand deposits above the Paleocene–Eocene TP2/TE1 sequence boundary. *Mississippi Geology* **11**, 9–14.
26. Case GR. 1994a Fossil fish remains from the late Paleocene Tuscahoma and early Eocene Bashi formations of Meridian, Lauderdale County, Mississippi. Part II. Teleosteans. *Palaeontographica Abteilung A* pp. 139–153.
27. Case GR. 1994b Fossil fish remains from the Late Paleocene Tuscahoma and Early Eocene Bashi Formations of Meridian, Lauderdale County, Mississippi Part I. Selachians. *Palaeontographica Abteilung A* pp. 97–138.
28. Case G. 1986 The bony fishes (teleosts) of the Tuscahoma and Bashi formations, early Eocene, Meridian, Lauderdale County, Mississippi. *Mississippi Geology* **6**, 6–8.
29. Holman J, Dockery III D, Case G. 1991 Paleogene snakes of Mississippi. *Mississippi Geology* **11**, 1–12.
30. Beard K, Tabrum A. 1991 The first early Eocene mammal from eastern North America: an omomyid primate from the Bashi Formation, Lauderdale County, Mississippi. *Mississippi Geology* **11**, 1–6.
31. Keating-Bitonti CR, Ivany LC, Affek HP, Douglas P, Samson SD. 2011 Warm, not super-hot, temperatures in the early Eocene subtropics. *Geology* **39**, 771–774.
32. Kobashi T, Grossman EL. 2003 The oxygen isotopic record of seasonality in Conus shells and its application to understanding late middle Eocene (38 Ma) climate. *Paleontological Research* **7**, 343–355.
33. Grossman EL, Ku TL. 1986 Oxygen and carbon isotope fractionation in biogenic aragonite: temperature effects. *Chemical Geology: Isotope Geoscience Section* **59**, 59–74.
34. Wilf P, Beard KC, Davies-Vollum KS, Norejko JW. 1998 Portrait of a late Paleocene (early Clarkforkian) terrestrial ecosystem; Big Multi Quarry and associated strata, Washakie Basin, southwestern Wyoming. *Palaios* **13**, 514–532.
35. Winkler DA. 1983 Paleoecology of an early Eocene mammalian fauna from paleosols in the Clarks Fork Basin, northwestern Wyoming (USA). *Palaeogeography, Palaeoclimatology, Palaeoecology* **43**, 261–298.
36. Breard SQ, Stringer GL. 1999 Abstract: Integrated Paleoecology and Marine Vertebrate Fauna of the Stone City Formation (Middle Eocene), Brazos River Section, Texas . *AAPG Bulletin* **83**.
37. Westgate JW. 2001 Paleoecology and biostratigraphy of marginal marine Gulf Coast Eocene vertebrate localities. In *Eocene biodiversity* , pp. 263–297. Springer.
38. Harding SC, Nash BP, Petersen EU, Ekdale A, Bradbury CD, Dyar MD. 2014 Mineralogy and geochemistry of the Main Glauconite Bed in the Middle Eocene of Texas: Paleoenvironmental implications for the Verdine Facies. *PloS one* **9**, e87656.
39. Flis JE, Yancey TE, Flis CJ. 2017 Middle Eocene Storm Deposition in the Northwestern Gulf of Mexico, Burleson County, Texas, U.S.A. *Gulf Coast Association of Geological Societies* **6**, 201–225.
40. Stanton Jr RJ, Nelson PC. 1980 Reconstruction of the trophic web in paleontology: community structure in the Stone City Formation (Middle Eocene, Texas). *Journal of Paleontology* pp. 118–135.
41. Zuschin M, Stanton Jr RJ. 2002 Paleocommunity reconstruction from shell beds: a case study from the Main Glauconite Bed, Eocene, Texas. *Palaios* **17**, 602–614.

42. Kneebone J, Chisholm J, Skomal GB. 2012 Seasonal residency, habitat use, and site fidelity of juvenile sand tiger sharks Carcharias taurus in a Massachusetts estuary. *Marine Ecology Progress Series* **471**, 165–181.
43. Teter SM, Wetherbee BM, Fox DA, Lam CH, Kiefer DA, Shivji M. 2015 Migratory patterns and habitat use of the sand tiger shark (Carcharias taurus) in the western North Atlantic. *Marine and Freshwater Research* **66**, 158–169.
44. Shimada K. 2002 Dental homologies in lamniform sharks (Chondrichthyes: Elasmobranchii). *Journal of Morphology* **251**, 38–72.
45. Goldman KJ, Branstetter S, Musick JA. 2006 A re-examination of the age and growth of sand tiger sharks, Carcharias taurus, in the western North Atlantic: The importance of ageing protocols and use of multiple back-calculation techniques. *Environmental Biology of Fishes* **77**, 241–252.
46. Cortés E, Parsons GR. 1996 Comparative demography of two populations of the bonnethead shark (Sphyrna tiburo). *Canadian Journal of Fisheries and Aquatic Sciences* **53**, 709–718.
47. Schindler DE, Essington TE, Kitchell JF, Boggs C, Hilborn R. 2002 Sharks and tunas: fisheries impacts on predators with contrasting life histories. *Ecological Applications* **12**, 735–748.
48. West GB, Brown JH, Enquist BJ. 2001 A general model for ontogenetic growth. *Nature* **413**, 628–631.
49. Moses ME, Hou C, Woodruff WH, West GB, Nekola JC, Zuo W, Brown JH. 2008 Revisiting a Model of Ontogenetic Growth: Estimating Model Parameters from Theory and Data. *http://dx.doi.org.proxy.lib.sfu.ca/10.1086/679735* **171**, 632–645.
50. Yeakel JD, Kempes CP, Redner S. 2018 Dynamics of starvation and recovery predict extinction risk and both DamuthâĂŹs law and CopeâĂŹs rule. *Nature communications* **9**, 1–10.
51. Brown JH, Gillooly JF, Allen AP, Savage VM, West GB. 2004 Toward a metabolic theory of ecology. *Ecology* **85**, 1771–1789.
52. Zeichner S, Colman A, Koch P, Polo-Silva C, Galván-Magaña F, Kim S. 2017 Discrimination factors and incorporation rates for organic matrix in shark teeth based on a captive feeding study. *Physiological and Biochemical Zoology* **90**, 257–272.
53. Haulsee D, Breece M, Brown L, Wetherbee B, Fox D, Oliver M. 2018 Spatial ecology of Carcharias taurus in the northwestern Mid-Atlantic coastal ocean. *Marine Ecology Progress Series* **597**, 191–206.
54. West CK, Greenwood DR, Reichgelt T, Lowe AJ, Vachon JM, Basinger JF. 2020 Paleobotanical proxies for early Eocene climates and ecosystems in northern North America from middle to high latitudes. *Climate of the Past* **16**, 1387–1410.
55. Zhu J, Poulsen CJ, Otto-Bliesner BL, Liu Z, Brady EC, Noone DC. 2020 Simulation of early Eocene water isotopes using an Earth system model and its implication for past climate reconstruction. *Earth and Planetary Science Letters* **537**, 116164.
56. West CK, Greenwood DR, Basinger JF. 2015 Was the Arctic Eocene âĂŸrainforestâĂŹmonsoonal? Estimates of seasonal precipitation from early Eocene megafloras from Ellesmere Island, Nunavut. *Earth and Planetary Science Letters* **427**, 18–30.
57. Heupel MR, Carlson JK, Simpfendorfer CA. 2007 Shark nursery areas: concepts, definition, characterization and assumptions. *Marine Ecology Progress Series* **337**, 287–297.
58. Heupel MR, Knip DM, Simpfendorfer CA, Dulvy NK. 2014 Sizing up the ecological role of sharks as predators. *Marine Ecology Progress Series* **495**, 291–298.